Effects of Unsymmetrical Stability Derivative Characteristics on Re-entry Vehicle Transient Angular Motion

Albert E. Hodapp Jr.*
Sandia Laboratories, Albuquerque, N. Mex.

A quasi-steady analytical theory is developed to investigate the effects that unsymmetrical stability derivative characteristics can have on the transient angular motion behavior of slender rolling re-entry vehicles. The theoretical results indicate that the presence of unsymmetrical stability derivatives can alter the motion patterns, frequency, and damping sufficiently to invalidate the use of previous analytical models developed for vehicles with symmetrical stability derivative characteristics. Between the resonances small asymmetries in the static moment slope coefficients are shown to cause a static instability which results in an exponential growth of the transient angle of attack. The analytically derived expressions and the analytically predicted trends are verified by numerical analyses.

Nomenclature

cg = center of gravity
C_A = axial force coefficient, $-F_X/q'S$
C_m = pitching moment coefficient, $M_Y/q'Sd$
C_{m_0} = aerodynamic asymmetry induced pitching moment coefficient
C_{m_q} = damping derivative coefficient, $\partial C_m/\partial(qd/2U)$, rad^{-1}
C_{m_α} = pitching moment slope coefficient, $\partial C_m/\partial\alpha$, rad^{-1}
$C_{m_{\dot\alpha}}$ = damping derivative coefficient, $\partial C_m/\partial(\dot\alpha d/2U)$, rad^{-1}
C_n = yawing moment coefficient, $M_Z/q'Sd$
C_{n_0} = aerodynamic asymmetry induced yawing moment coefficient
C_{n_r} = damping derivative coefficient, $\partial C_n/\partial(rd/2U)$, rad^{-1}
C_{n_β} = yawing moment slope coefficient, $\partial C_n/\partial\beta$, rad^{-1}
$C_{n_{\dot\beta}}$ = damping derivative coefficient $\partial C_n/\partial(\dot\beta d/2U)$, rad^{-1}
C_Y = force coefficient for Y-body direction, $F_Y/q'S$
C_{Y_β} = force slope coefficient, $\partial C_Y/\partial\beta$, rad^{-1}
C_Z = force coefficient for Z-body direction, $F_Z/q'S$
C_{Z_α} = force slope coefficient, $\partial C_Z/\partial\alpha$, rad^{-1}
d = vehicle base diameter (Fig. 1), ft or m
F_X,F_Y,F_Z = aerodynamic forces acting along the X,Y,Z axes, respectively, lb or N
G = critical frequency ratio [Eq. (12)]
h = altitude, ft or m
i = $(-1)^{1/2}$
I_X,I_Y,I_Z = moments of inertia about the X,Y,Z axes, respectively, slug-ft^2 or kg-m^2
J_{XY},J_{YZ},J_{XZ} = products of inertia relative to the X,Y,Z axes, slug-ft^2 or kg-m^2
m = vehicle mass, slugs or kg
m_j = jth root of Eq. (7), sec^{-1}
M_X,M_Y,M_Z = aerodynamic moments about the X,Y,Z axes, respectively, ft-lb or N-m
p,q,r = angular velocities about the X,Y,Z axes, respectively (roll, ptich and yaw rates), rad/sec
$p_{\text{crp}},p_{\text{cry}}$ = pitch and yaw critical frequencies, respectively, [Eqs. (15) and (16)], rad/sec
q' = dynamic pressure, lb/ft^2 or N/m^2
S = reference area, $S=\pi d^2/4$, ft^2 or m^2
t = time, sec
U = total velocity, fps or m/sec
X,Y,Z = body reference axes, mutually parallel to X_g,Y_g,Z_g axes, with origin at the cg (Fig. 1)
X_g,Y_g,Z_g = geometric axes, with X_g the axis of basic geometric symmetry (Fig. 1)
X_p,Y_p,Z_p = principal axes (Fig. 1)
$y_{\text{cg}},z_{\text{cg}}$ = position of the cg relative to origin of X_g,Y_g,Z_g axes along Y_g and Z_g axes, respectively (Fig. 1), ft or m
α,β = angle of attack and side-slip angle, respectively, rad or deg
γ = flight-path angle, deg
$\delta_\alpha,\delta_\beta$ = inclinitation angles between the X_p,Y_p,Z_p and X,Y,Z axes [Fig. 1 and Eqs. (1) and (2)], rad or deg
ζ = complex total angle of attack [Eq. (38)], rad or deg
θ_2,ψ_1 = static and dynamic stability criterion [Eq. (39)], respectively, 1/sec^4 and 1/sec^3
$\lambda_0,\Delta\lambda,\lambda_A$ = contributions to damping rates from aerodynamic damping, roll rate, and unsymmetrical stability derivatives, respectively [Eqs. (31) and (32)], sec^{-1}

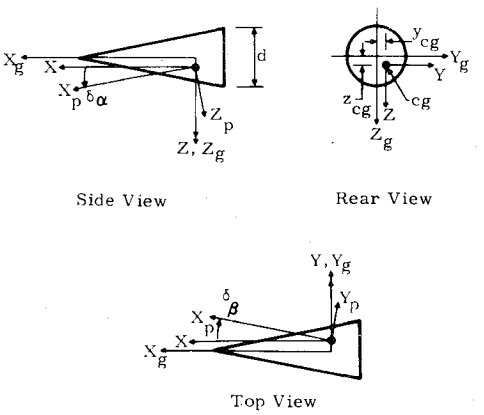

Fig. 1 Coordinate systems and nomenclature. Note: δ_α and δ_β are shown for $J_{YZ}=0$.

Received May 22, 1975; revision received August 11, 1975. This work was supported by the U.S. Energy Research and Development Administration. The author wishes to thank G. E. Reis, W. E. Williamson, and J. R. Kelsey of Sandia Laboratories for their assistance and suggestions.

Index categories: Entry Vehicle Dynamics and Control; LV/M Dynamics and Control.

*Member of the Technical Staff, Aerodynamics Projects Department. Member AIAA.

λ_p, λ_y = pitch and yaw roll rate ratios, respectively [Eqs. (13) and (14)]
$\lambda_s, \lambda_f, \lambda_j$ = damping rate of slow, fast, and jth rotating vector, respectively [Eqs. (27) through (32)], sec^{-1}
μ_p, μ_y = pitch and yaw damping ratios, respectively [Eqs. (17) and (18)]
ρ = atmospheric density, $slug/ft^3$ or kg/m^3
$\omega_0, \Delta\omega, \omega_A$ = contributions to circular frequencies from aerodynamic frequency, roll rate, and unsymmetrical stability derivatives, respectively [Eqs. (33) and (34)], rad/sec
$\omega_s, \omega_f, \omega_j$ = circular frequencies of slow, fast, and jth rotating vector, respectively [Eqs. (27) through (30), (33) and (34)], rad/sec
$| \; |$ = absolute value or magnitude
$(\cdot), (\cdot\cdot)$ = first and second derivatives with respect to time

Subscripts

i, T = initial and trim conditions
I, R = imaginary and real parts

Introduction

MANY descriptions of the transient angular motion of rolling missiles can be found in the literature, including those by Nicolaides,[1] Murphy,[2] and Nelson,[3] which are widely referenced. Although many of these descriptions include the effects of small trim producing asymmetries, most use the assumption that the stability derivative characteristics of the missile are symmetrical; i.e., $C_{Z_\alpha} = C_{Y_\beta}$, $C_{m_\alpha} = -C_{n_\beta}$, $C_{m_q} + C_{m_{\dot\alpha}} = C_{n_r} - C_{n_{\dot\beta}}$, etc. Phillips[4] presented descriptions of transient angular motion for rolling airplanes which include effects of unsymmetrical stability derivative characteristics ($C_{Z_\alpha} \neq C_{Y_\beta}, C_{m_\alpha} \neq -C_{n_\beta}, C_{m_q} + C_{m_{\dot\alpha}} \neq C_{n_r} - C_{n_{\dot\beta}}$, etc.). More recently Regan[5] did the same for spinning tail rolling missiles. To the author's knowledge, descriptions of the effects that unsymmetrical stability derivatives have on the transient angular motions of slender rolling re-entry vehicles have not appeared in the literature. Walchner[6] has shown experimentally that at hypersonic speeds small nosetip asymmetries on otherwise symmetrical conical vehicles can introduce flowfield pressure perturbations which, in addition to creating trim angles, invalidate the symmetrical aerodynamic stability derivative assumption. Since nosetip asymmetries can occur during re-entry flight, an understanding of these effects on angular motion is desirable. The effects that unsymmetrical stability derivative characteristics have on the trim angle behavior of slender rolling re-entry vehicles were presented in Ref. 7. A detailed description is given herein of the effects that unsymmetrical stability derivatives have on the transient angular motions of these vehicles. It is shown that the presence of unsymmetrical stability derivatives can alter the transient angular motion behavior sufficiently to invalidate descriptions of angular motion based on previous analytical results for re-entry vehicles. In addition to introducing changes in the motion, damping, and frequency throughout the flight regime, unsymmetrical stability derivatives can cause an instability in transient angular motion for flight conditions within the resonance region. Relative to the angular motions of vehicles with symmetrical stability derivatives, this instability in transient angular motion, which increases the likelihood for the occurrence of oscillatory roll resonance,[8] together with the increased trim magnification[7] combine to greatly increase the instability in angular motion behavior near resonance.

A quasi-steady analytical theory is developed to provide an insight into the effects that unsymmetrical stability derivative characteristics have on the transient angular motions of slender, rolling re-entry vehicles. As in previous investigations,[4,5] a fourth-order polynomial (quartic) characteristic equation is used to investigate vehicle stability boundaries using a Routh array; however, unlike previous efforts the complete quartic is solved to obtain the damping as well as the frequency expressions. The accuracy of the analytical expressions for damping and frequency is established by comparison with results obtained through a numerical analysis of the differential equations of motion and their characteristic equation. Numerical six-degree-of-freedom (6-DOF) simulations are presented to confirm the analytically predicted trends concerning the transient angular motion instability near resonance. The solution presented herein is developed for body fixed coordinates as was Nelson's solution[3] for missiles with symmetrical aerodynamic characteristics. The changes in the motion, damping, and frequency introduced by the presence of unsymmetrical stability derivative characteristics are illustrated by comparison with Nelson's results.

Theoretical Analysis

Equations of Angular Motion

The following linear differential equations describe the pitching-yawing motions of a rolling re-entry vehicle that has unsymmetrical stability derivative characteristics and small mass, aerodynamic, and inertia asymmetries

$$\ddot\alpha + A_\alpha\dot\alpha + B_\alpha\alpha + C_\alpha\ddot\beta + D_\alpha\dot\beta + E_\alpha\beta = F_\alpha \tag{1}$$

where

$$A_\alpha = -\left(\frac{q'S}{mU}\right)\left[(C_A + C_{Z_\alpha}) + \frac{md^2}{2I_Y}(C_{m_q} + C_{m_{\dot\alpha}})\right]$$

$$B_\alpha = -\frac{q'Sd}{I_Y}C_{m_\alpha} - \left[\frac{I_Z - I_X}{I_Y}\right]p^2$$

$$C_\alpha = J_{YZ}/I_Y$$

$$D_\alpha = p\left[1 + \left(\frac{I_Z - I_X}{I_Y}\right)\right]$$

$$E_\alpha = -p\left(\frac{q'S}{mU}\right)\left[\left(\frac{I_Z - I_X}{I_Y}\right)(C_A + C_{Y_\beta}) + \frac{md^2}{2I_Y}C_{m_q}\right] + \frac{J_{YZ}}{I_Y}p^2$$

$$F_\alpha = \frac{q'Sd}{I_Y}\left[C_{m_0} + C_A\left(\frac{z_{cg}}{d}\right)\right] - \left[\frac{I_Z - I_X}{I_Y}\right]\delta_\alpha p^2$$

$$\delta_\alpha = J_{XZ}/(I_Z - I_X)$$

and

$$\ddot\beta + A_\beta\dot\beta + B_\beta\beta + C_\beta\ddot\alpha + D_\beta\dot\alpha + E_\beta\alpha = F_\beta \tag{2}$$

where

$$A_\beta = -\left(\frac{q'S}{mU}\right)\left[(C_A + C_{Y_\beta}) + \frac{md^2}{2I_Z}(C_{n_r} - C_{n_{\dot\beta}})\right]$$

$$B_\beta = \frac{q'Sd}{I_Z}C_{n_\beta} - \left[\frac{I_Y - I_X}{I_Z}\right]p^2$$

$$C_\beta = J_{YZ}/I_Z$$

$$D_\beta = -p\left[1 + \left(\frac{I_Y - I_X}{I_Z}\right)\right]$$

$$E_\beta = p\left(\frac{q'S}{mU}\right)\left[\left(\frac{I_Y - I_X}{I_Z}\right)(C_A + C_{Z_\alpha}) + \frac{md^2}{2I_Z}C_{n_r}\right] + \frac{J_{YZ}}{I_Z}p^2$$

$$F_\beta = -\frac{q'Sd}{I_Z}\left[C_{n_0} - C_A\left(\frac{y_{cg}}{d}\right)\right] - \left[\frac{I_Y - I_X}{I_Z}\right]\delta_\beta p^2$$

$$\delta_\beta = J_{XY}/(I_Y - I_X)$$

These coupled differential equations were derived using the X, Y, Z body fixed axis system (Fig. 1) as a reference. The assumptions used in developing the equations are as follows: a) Gravitational acceleration and asymmetry induced forces have a negligible effect on the angular motions of the re-entry vehicle; b) The re-entry vehicle experiences only small perturbations in angle of attack and side-slip angle (α and $\beta \ll 1$ rad.); c) Aerodynamic forces and moments vary linearly with α, β, q, r, and the time derivatives of α and β; d) The products of inertia J_{XY}, J_{XZ}, and J_{YZ} are small compared to the moments of inertia I_X, I_Y, and I_Z; and e) Mass and aerodynamic asymmetries are small ($|y_{cg}/d|$ and $|z_{cg}/d| \ll 1$; $|C_{m_0}/C_{m_\alpha}|$ and $|C_{n_0}/C_{n_\beta}| \ll 1$).

During flight the coefficients of Eqs. (1) and (2) are variables because of altitude and velocity changes. For the quasi-steady theoretical results presented here, it is assumed that the variation of these coefficients with respect to time is such that they can be considered essentially constant over small time intervals of the flight. The quasi-steady trim angles or particular solutions of Eqs. (1) and (2) were obtained previously.[7] The homogeneous solutions, which describe the quasi-steady transient angular motions, are being sought in this development. The homogeneous portions of the governing differential equations, Eqs. (1) and (2), are given as

$$\ddot{\alpha} + A_\alpha\dot{\alpha} + B_\alpha\alpha + C_\alpha\ddot{\beta} + D_\alpha\dot{\beta} + E_\alpha\beta = 0 \tag{3}$$

$$\ddot{\beta} + A_\beta\dot{\beta} + B_\beta\beta + C_\beta\ddot{\alpha} + D_\beta\dot{\alpha} + E_\beta\alpha = 0 \tag{4}$$

where the coefficients of Eqs. (3) and (4) are defined in Eqs. (1) and (2). The homogeneous trial solutions are given as

$$\alpha = \sum_{j=1}^{4} K_j e^{m_j t} \tag{5}$$

$$\beta = \sum_{j=1}^{4} H_j e^{m_j t} \tag{6}$$

where K_j and H_j are constants determined by the initial conditions and Eq. (1) or Eq. (2), and m_j represents the eigenvalues of the dynamic system. In the following development, the eigenvalues will be manipulated to obtain the frequency and damping expressions for the system.

A consequence of assuming that the coefficients of Eqs. (1) and (2) are constant is that Eqs. (5) and (6) describe the steady-state transient angular motion (solutions of time-invariant differential equations). This ignores a sometimes large effect on total angle-of-attack convergence or divergence which results from changes in total velocity, U, and aerodynamic frequency, ω_0, as the vehicle descends through the atmosphere. Corrections can be derived which account approximately for these effects; however, these corrections are a complete subject by themselves and are not dealt with in this paper. The present discussion is confined to describing basic effects introduced by the presence of unsymmetrical stability derivatives which change the motion patterns, damping, and frequency relative to those for vehicles with symmetrical stability derivative coefficients.

Damping and Frequency

Substituting Eqs. (5) and (6) and their derivatives into Eqs. (3) and (4) yields

$$K_j(m_j^2 + A_\alpha m_j + B_\alpha) + H_j(C_\alpha m_j^2 + D_\alpha m_j + E_\alpha) = 0$$

$$K_j(C_\beta m_j^2 + D_\beta m_j + E_\beta) + H_j(m_j^2 + A_\beta m_j + B_\beta) = 0$$

In order for this system of equations to have a nontrivial solution, the determinant of the coefficients of K_j and H_j must vanish. The characteristic equation for the dynamic system [Eqs. (1) and (2)] obtained by expanding the resultant determinant is given as

$$m_j^4 + cm_j^3 + fm_j^2 + km_j + \ell = 0 \tag{7}$$

where

$$c = A_\alpha + A_\beta$$

$$f = B_\alpha + B_\beta + A_\alpha A_\beta - D_\alpha D_\beta$$

$$k = A_\alpha B_\beta + A_\beta B_\alpha - D_\alpha E_\beta - D_\beta E_\alpha$$

$$\ell = B_\alpha B_\beta - E_\alpha E_\beta$$

The coefficients of Eq. (7) have been reduced somewhat in form by neglecting products which contain the terms C_α or c_β. According to the assumption (d), C_α and $C_\beta \ll 1$.

The B_α, B_β, E_α, and E_β coefficients of Eqs. (1, 2, and 7) are expressed in terms of the roll rate ratios (λ_p and λ_y) and damping ratios (μ_p and μ_y) of Ref. 7 as

$$B_\alpha = p^2\left[\frac{I_Z - I_X}{I_Y}\right]\left[\frac{1}{\lambda_p^2} - 1\right] \tag{8}$$

$$B_\beta = p^2\left[\frac{I_Y - I_X}{I_Z}\right]\left[\frac{1}{G^2\lambda_p^2} - 1\right] \tag{9}$$

$$E_\alpha = p\left[\frac{I_Z - I_X}{I_Y}\right] p_{crp}\mu_p \tag{10}$$

$$E_\beta = -p\left[\frac{I_Y - I_X}{I_Z}\right] p_{cry}\mu_y \tag{11}$$

where the critical frequency ratio G (a constant) is given as

$$G = \frac{\lambda_y}{\lambda_p} = \left[\frac{-C_{m_\alpha}(I_Y - I_X)}{C_{n_\beta}(I_Z - I_X)}\right]^{1/2} \tag{12}$$

and

$$\lambda_p = p/p_{crp} \tag{13}$$

$$\lambda_y = p/p_{cry} \tag{14}$$

$$p_{crp} = \pm\left[-C_{m_\alpha}\, q'Sd/(I_Z - I_X)\right]^{1/2} \tag{15}$$

$$p_{cry} = \pm\left[C_{n_\beta}\, q'Sd/(I_Y - I_X)\right]^{1/2} \tag{16}$$

$$\mu_p = \pm\left\{-\rho^{1/2}S\left[\frac{1}{2m}(C_A + C_{Y_\beta}) + \frac{d^2}{4}\left[\frac{C_{m_q}}{I_Z - I_X}\right]\right] \Big/ \left[\frac{-C_{m_\alpha}Sd}{2(I_Z - I_X)}\right]^{1/2}\right\} \tag{17}$$

$$\mu_y = \pm\left\{-\rho^{1/2}S\left[\frac{1}{2m}(C_A + C_{Z_\alpha}) + \frac{d^2}{4}\left[\frac{C_{n_r}}{I_Y - I_X}\right]\right] \Big/ \left[\frac{C_{n_\beta}Sd}{2(I_Y - I_X)}\right]^{1/2}\right\} \tag{18}$$

The signs of the pitch and yaw critical frequencies p_{crp} and p_{cry} are the same as that of p; therefore, the roll rate ratios λ_p and λ_y are always positive. Similarly, the signs outside the brackets in the expressions for the damping ratios μ_p and μ_y are the same as that of p. The aerodynamic terms combine to yield a positive term within the brackets of Eqs. (17) and (18) for re-entry configurations of interest; then μ_p and μ_y have the sign of the roll rate.

In order to reduce Eq. (7) to biquadratic form, the substitution

$$m_j = z_j - \frac{c}{4} \tag{19}$$

is used. This suppresses the cubic term and reduces Eq. (7) to

$$z_j^4 + \Lambda z_j^2 + \Omega z_j + \Gamma = 0 \tag{20}$$

where

$$\Lambda = f - 6\left(\frac{c}{4}\right)^2$$

$$\Omega = 8\left(\frac{c}{4}\right)^3 - 2f\left(\frac{c}{4}\right) + k$$

$$\Gamma = \ell + f\left(\frac{c}{4}\right)^2 - 3\left(\frac{c}{4}\right)^4 - k\left(\frac{c}{4}\right)$$

The first and zeroth order terms of Eq. (20) are transposed, and $az_j^2 + b$ is added to both sides of the resulting equation. The following forms of a and b are chosen to make both sides of this equation perfect squares.

$$b = \left[\frac{(a+\Lambda)}{2}\right]^2 \tag{21}$$

and

$$\frac{(b-\Gamma)}{a} = \left[\frac{\Omega}{2a}\right]^2 \tag{22}$$

Factoring the squares on both sides of the equation and taking the square root gives two quadratic equations. These equations are solved to obtain

$$z_{1,2} = \frac{1}{2}\left[a^{1/2} \pm i\left(a + 2\Lambda + \frac{2\Omega}{a^{1/2}}\right)^{1/2}\right] \tag{23}$$

$$z_{3,4} = \frac{1}{2}\left[-a^{1/2} \pm i\left(a + 2\Lambda - \frac{2\Omega}{a^{1/2}}\right)^{1/2}\right] \tag{24}$$

The resolvent cubic equation, from which a is determined, is obtained using Eqs. (21) and (22).

$$a^3 + 2\Lambda a^2 + [\Lambda^2 - 4\Gamma]a - \Omega^2 = 0 \tag{25}$$

Any solution of this equation can be substituted into Eqs. (23) and (24) to obtain the four roots of Eq. (20). In dealing with Eq. (25), it was observed that the effects of aerodynamic damping were secondary. This suggested a perturbation approach through which the following approximate solution was obtained.

$$a \approx -\Lambda + 2\Gamma^{1/2} + \frac{\Omega^2}{4\Gamma^{1/2}(-\Lambda + 2\Gamma^{1/2})} \tag{26}$$

Substituting Eq. (26) into Eqs. (23) and (24) and ignoring small terms,

$$z_{1,2} = \left[\frac{\Gamma^{1/2} - (1/2)\Lambda}{2}\right]^{1/2} \pm i\left[\frac{\Gamma^{1/2} + (1/2)\Lambda}{2}\right]^{1/2} \times \left[1 + \frac{\Omega}{\{2[\Gamma^{1/2} - (1/2)\Lambda]\}^{1/2}[\Gamma^{1/2} + (1/2)\Lambda]}\right]^{1/2}$$

$$z_{3,4} = -\left[\frac{\Gamma^{1/2} - (1/2)\Lambda}{2}\right]^{1/2} \pm i\left[\frac{\Gamma^{1/2} + (1/2)\Lambda}{2}\right]^{1/2} \times \left[1 - \frac{\Omega}{\{2[\Gamma^{1/2} - (1/2)\Lambda]\}^{1/2}[\Gamma^{1/2} + (1/2)\Lambda]}\right]^{1/2}$$

Because the terms involving Ω in both of the above expressions are small compared to one, the binomial theorem can be used to expand the radicals containing these terms. Substituting the above equations into Eq. (19), expanding the radicals, and factoring the result yields

$$m_1 = \lambda_f + i\omega_f = \lambda_1 + i\omega_1 \tag{27}$$

$$m_2 = \lambda_s + i\omega_s = \lambda_2 + i\omega_2 \tag{28}$$

$$m_3 = \lambda_s - i\omega_s = \lambda_3 + i\omega_3 \tag{29}$$

$$m_4 = \lambda_f - i\omega_f = \lambda_4 + i\omega_4 \tag{30}$$

where

$$\lambda_f = -\frac{c}{4} + \frac{\Omega}{2[\Lambda^2 - 4\Gamma]^{1/2}}$$

$$\lambda_s = -\frac{c}{4} - \frac{\Omega}{2[\Lambda^2 - 4\Gamma]^{1/2}}$$

$$\omega_f = \left\{(1/2)\Lambda + \frac{1}{2}[\Lambda^2 - 4\Gamma]^{1/2}\right\}^{1/2}$$

$$\omega_s = \left\{(1/2)\Lambda - \frac{1}{2}[\Lambda^2 - 4\Gamma]^{1/2}\right\}^{1/2}$$

The f and s subscripts denote components of the fast and slow rotating vectors similar to those identified by Nelson.[3] Note that m_1 and m_4 are complex conjugates, as are m_2 and m_3.

The damping and frequency expressions are obtained as functions of the coefficients of Eqs. (1) and (2) by substituting the expressions for the coefficients of Eqs. (7) and (20) into Eqs. (27) through Eq. (30). Factoring these expressions and neglecting small terms yields

$$\lambda_f = \lambda_0 - \Delta\lambda - \lambda_A \tag{31}$$

$$\lambda_s = \lambda_0 + \Delta\lambda + \lambda_A \tag{32}$$

$$\omega_f = [(\omega_0 + \Delta\omega)^2 + \omega_A]^{1/2} \tag{33}$$

$$\omega_s = [(\omega_0 - \Delta\omega)^2 + \omega_A]^{1/2} \tag{34}$$

where

$$\lambda_0 = -1/4(A_\alpha + A_\beta)$$

$$\Delta\lambda = \frac{-D_\alpha D_\beta(A_\alpha + A_\beta) + 2(D_\alpha E_\beta + D_\beta E_\alpha)}{16\omega_0(\Delta\omega)}$$

$$\lambda_A = \frac{-(B_\alpha - B_\beta)(A_\beta - A_\alpha)}{16\omega_0(\Delta\omega)}$$

$$\omega_0 = \left[\frac{(B_\alpha + B_\beta)}{2} - \frac{D_\alpha D_\beta}{4} - \omega_A\right]^{1/2}$$

$$\Delta\omega = \frac{[-D_\alpha D_\beta]^{1/2}}{2}$$

$$\omega_A = \frac{-(B_\alpha - B_\beta)^2}{16(\Delta\omega)^2}$$

The damping and frequency terms given above are similar to those derived by Nelson,[3] with the exception of the A subscripted terms which are introduced by the presence of unsymmetrical stability derivative characteristics. If symmetrical stability derivatives and equal lateral moments of inertia are used, the A subscripted terms vanish and the expressions reduce to Nelson's results.

For flight conditions within the resonance region, as discussed later, the ω_A term (a differencing of the B_α and B_β coefficients) together with the averaging of the unequal B_α and B_β coefficients become the dominant effects on both damping and frequency. For rolling vehicles at conditions away from resonance, the effects of both the ω_A term on frequency and the λ_A term on damping appear to be small; however, even for small asymmetries in the stability derivatives the λ_A and ω_A terms cannot be ignored when the previous expressions are used to extract the stability derivative coefficients from experimental data. When $p \to 0$, the damping and frequency terms [Eqs. (31-34)] remain bounded and well behaved while ω_A diverges.

Biased averages of the correct stability derivative coefficients result when data reduction models developed for symmetrical rolling vehicles are applied to data which contain effects generated by unsymmetrical stability derivatives. The biasing takes place because the analytical results for symmetrical vehicles do not account for the λ_A and ω_A terms. As an example, consider evaluating the static moment slope coefficients of a vehicle with $G=1.15$ and $(-C_{m_\alpha}+C_{n_\beta})/2.0=0.31$ using Nelson's analytical model[3] which was developed for symmetrical missiles. This would yield the incorrect average $-C_{m_\alpha}=C_{n_\beta}=0.327$, which overestimates the minimum static margin by 22.5% ($C_{n_\beta}=0.267$) and underestimates the maximum static margin by 7.4% ($C_{m_\alpha}=-0.353$).

Total Angle of Attack

Summing the expressions for the particular solutions (α_T and β_T) derived previously in Ref. 7 together with the appropriate homogeneous solution, Eqs. (5) and (6), the complete quasi-steady solution to the system of equations, Eqs. (1) and (2), is given as

$$\alpha = \sum_{j=1}^{4} K_j e^{m_j t} + \alpha_T \tag{35}$$

$$\beta = \sum_{j=1}^{4} H_j e^{m_j t} + \beta_T \tag{36}$$

Note that the solutions, Eqs. (35) and (36), contain eight arbitrary constants (the summations from 1 to 4 on both K_j and H_j) when four are required. To determine the relationship between the constants H_j and K_j, Eqs. (35) and (36) were substituted into Eq. (1). Assuming that $C_\alpha \approx C_\beta \approx 0$, this results in

$$K_j = H_j F_j = (H_{R_j} + iH_{I_j})\ (F_{R_j} + iF_{I_j}) \tag{37}$$

where

$$F_j = \frac{-(D_\alpha m_j + E_\alpha)}{(m_j^2 + A_\alpha m_j + B_\alpha)}$$

Therefore, as required, the solutions to Eqs. (1) and (2) contain only four arbitrary constants.

Using Eqs. (35-37) along with the four initial conditions provided by α, β, and their time derivatives, the solutions for the complex constants H_j can be obtained. From the resulting system of eight simultaneous linear equations, it was determined that the coefficients H_1 and H_4 are complex conjugates as are H_2 and H_3.

The complex total angle of attack ζ can be defined in terms of α, β [Eq. (35) and (36)], and Eq. (37) as follows:

$$\zeta = \beta + i\alpha = \sum_{j=1}^{4} H_j (1 + iF_j) e^{(\lambda_j + i\omega_j)t} + \zeta_T \tag{38}$$

Equation (38) indicates that the total angle of attack is described by four rotating transient vectors and one trim vector. The position and magnitude of the trim vector ζ_T, described in Ref. 7, are functions of the critical frequency ratio G and roll rate ratio λ_p and not functions of time. When the stability derivatives of the vehicle are symmetrical, Eq. (38) reduces to the model described by Nelson,[3] which has a trim vector and two rotating transient vectors.

Asymmetries in the static force slope coefficients and damping derivative coefficients cause small changes in total transient angle of attack behavior through their effect on the damping rates λ_s and λ_f; however, the dominant effect of unsymmetrical stability derivative coefficient characteristics on transient angular motion is that which results from differences in the pitching moment slope and yawing moment slope coefficient (i.e., when $C_{m_\alpha} \neq -C_{n_\beta}$). This effect is illustrated in Fig. 2 by comparing a motion pattern for a vehicle with symmetrical static moment slope characteristics (Fig. 2a, $G=1.0$) to motion patterns generated by vehicles with unsymmetrical static moment slope coefficients (Figs. 2b, c, and d; $G=1.05$, 1.10, and 1.15). With the exception of the static moment slope coefficients, which have the same average values for each vehicle, all other characteristics of these vehicles are identical, as are the initial conditions of the motion.

The angular motion patterns shown in Fig. 2 are similar; however, it is obvious from the looped and rounded apexes of the triangular motion in Figs. 2b, c, and d that the angular motion patterns for the vehicles with unsymmetrical static moment slope characteristics ($G>1.0$, Fig. 2) contain additional contributions. These perturbations increase in magnitude as the asymmetry in the static moment slope coefficients increases. Note in Fig. 2 that the clockwise rotation rate of the triangular motion in the $i\alpha-\beta$ plane is highest for the vehicle with symmetrical static moment slope characteristics ($G=1.0$). The difference in the rotation rates of the motion patterns in Fig. 2 is caused by the effect that unsymmetrical stability derivatives have on changing the circular frequencies (ω_s and ω_f).

Stability

To investigate the stability of the quasi-steady motions of slender rolling re-entry vehicles, the Routh array presented below was formed from the characteristic equation [Eq. (7)] for the system

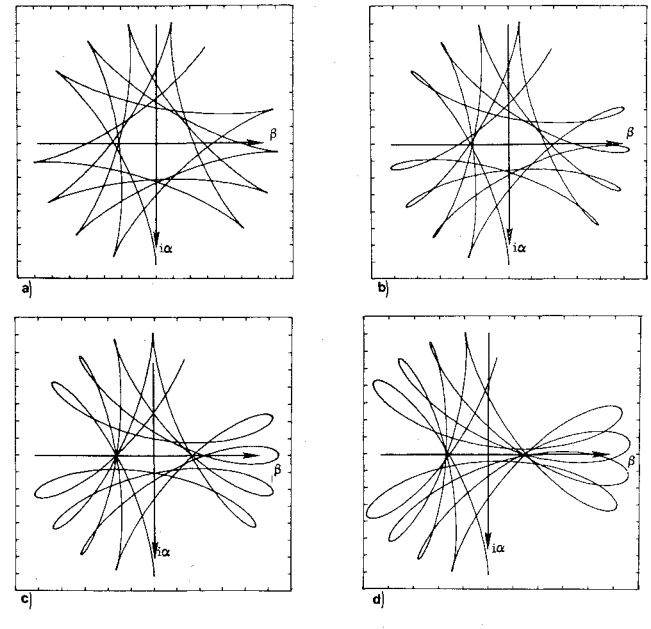

Fig. 2 Influence of static moment slope asymmetry on motion patterns: a) $G=1.00$; b) $G=1.05$; c) $G=1.10$; d) $G=1.15$.

$$\begin{array}{c|ccc} & & & \\ \hline m_j^4 & 1 & f & \ell \\ m_j^3 & c & k & 0 \\ m_j^2 & \theta_1 & \theta_2 & 0 \\ m_j & \psi_1 & 0 & 0 \\ m_j^0 & \theta_2 & 0 & 0 \end{array} \qquad (39)$$

where $\theta_1 = f - (k/c)$, $\theta_2 = \ell$, and $\psi_1 = k - (c\ell/\theta_1)$. According to the Routh stability criterion, if all the elements of the first column of the array [Eq. (39)] remain positive and nonzero then the real parts of the characteristic equation's roots [Eqs. (27-30)] remain negative (stable system). Each change in sign of the elements in the first column of the array indicates a root of the characteristic equation with a positive real part (unstable system). Over the flight regime of the re-entry vehicle, the coefficients of Eq. (7) vary with altitude, velocity, and roll rate; therefore, the elements of the Routh array are functions of these variables. It can be shown[5,9] that the system is stable if $c, f, k, \ell > 0$ [coefficients of Eq. (7)], and if $cfk - k^2 - c^2\ell > 0$. The last of these criteria is the dynamic stability criterion $\psi_1 > 0$ [Eq. (39)], and the static stability criterion is given as $\theta_2 = \ell > 0$.

The transient vectors of Eq. (38) can experience two types of instability; these are exponential divergence (static instability), where one or more real roots of the characteristic equation become positive, and oscillatory exponential divergence (dynamic instability), where the real part of one or more complex roots become positive. Boundaries for these instabilities are derived from the Routh criterion as $\theta_2 = 0$ for static instability and $\psi_1 = 0$ for dynamic instability. The vehicles considered herein have C_{m_α}, $-C_{n_\beta}$, C_{m_q}, C_{n_r}, etc., < 0; therefore, the term's static instability and dynamic instability do not indicate conditions which result from the presence of stability derivative coefficients with unfavorable signs. It should be recalled from an an earlier discussion that changing velocity and aerodynamic frequency have an effect on the convergence or divergence of the motion which is ignored by the quasi-steady solution; therefore, the above stability criteria cannot be considered absolute.

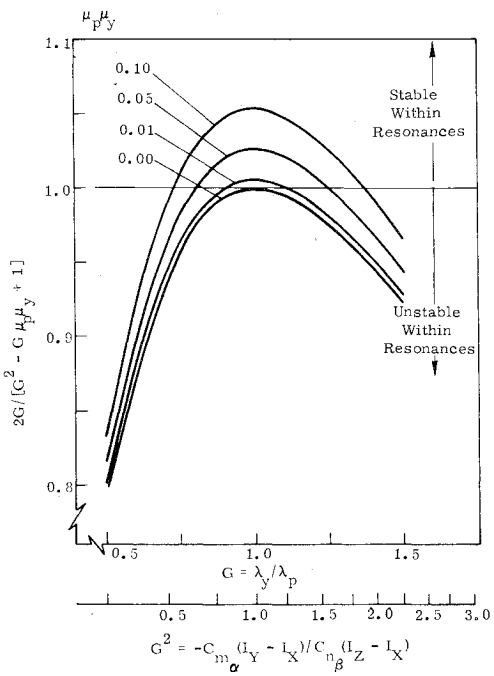

Fig. 3 Parameters which influence static stability within resonance region.

For the slender vehicles of interest with unsymmetrical stability derivatives, all coefficients of Eq. (7) with the exception of ℓ remain positive throughout the flight regime; i.e., the static stability criterion $\theta_2 > 0$ is not always satisfied. The dynamic stability criterion is satisfied for roll rates that are not large when compared to ω_0. As shown by Eq. (31) and (32), for large roll rates $\Delta\lambda$ can become dominant, thereby causing a dynamic instability (λ_s or $\lambda_f > 0$). This effect of roll rate on dynamic instability is well known; however, the presence of unsymmetrical stability derivatives does modify it somewhat. The failure of the static stability criterion is unexpected because it does not occur for vehicles with symmetrical stability derivative characteristics and equal lateral moments of inertia.

To determine the boundaries for the occurrence of static instability, Eqs. (8-18) were substituted into the expression for θ_2 [Eqs. (39) and (7)] and the result was equated to zero. This yields the following quartic equation in which the roll rate ratio λ_p is the independent variable.

$$\theta_2 = \lambda_p^4 - \left\{ \frac{G^2 - G\mu_p\mu_y + 1}{G^2} \right\} \lambda_p^2 + \frac{1}{G^2} = 0 \qquad (40)$$

when positive real roots of Eq. (40) exist, they must satisfy

$$\lambda_p = \frac{1}{G} \left\{ \frac{G^2 - G\mu_p\mu_y + 1}{G^2} \right\}^{1/2} \times \left\{ 1 \pm \left[1 - \left\{ \frac{2G}{G^2 - G\mu_p\mu_y + 1} \right\}^2 \right]^{1/2} \right\}^{1/2} \qquad (41)$$

Since G and the product $\mu_p\mu_y$ are both positive, with $\mu_p\mu_y \ll 1$, this equation indicates that when

$$2G/(G^2 - G\mu_p\mu_y + 1) \leq 1 \qquad (42)$$

a pair of real roots are obtained; therefore, zeroes of θ_2 result. For re-entry vehicles, these zeroes occur between the undamped resonance conditions $\lambda_p = 1$ and $\lambda_y = G\lambda_p = 1$. In the region between the zeroes defined by Eq. (41), the vehicle becomes statically unstable.

The product of damping ratios $\mu_p\mu_y$ [Eqs. (17) and (18)] has a strong influence on the range of G over which the vehicle remains statically stable near resonance. This is shown in Fig. 3 where the left hand side of Eq. (42) is plotted vs G for selected values of $\mu_p\mu_y$. According to Eq. (42), the horizontal line on Fig. 3 separates the regions of static stability (imaginary λ_p above the line) and static instability (positive real λ_p at and below the line). Each member of the family of curves ($\mu_p\mu_y = \text{const}$) presented in Fig. 3 intersects this horizontal line. The distance along the line between intersections defines the range of G over which the vehicle will remain statically stable as λ_p varies. Notice that as the magnitude of the product $\mu_p\mu_y$ increases, this range of G increases. Equations (17) and (18) show that μ_p and μ_y are directly proportional to $\rho^{1/2}$; therefore, as altitude decreases μ_p and μ_y increase in magnitude. Consequently, the range of

Table 1 Comparison of analytical and numerical results ($G = 1.15$)

	Analytical results Eqs. (32) and (34)		Results of numerical analysis	
h (ft $\times 10^{-3}$)	λ_s (sec^{-1})	ω_s (rad/sec)	λ_s (sec^{-1})	ω_s (rad/sec)
200	−0.0043350	13.039	−0.0043350	13.039
150	−0.036301	4.1384	−0.036301	4.1381
100	−0.29503	−19.794	−0.29503	−19.791
75	−0.79642	−41.701	−0.79642	−41.691
50	−1.8792	−64.432	−1.8792	−64.400
25	−3.0028	−59.446	−3.0028	−59.354
5	−2.0765	−17.256	−2.0765	−17.068

G for static stability within the resonance region increases with decreasing altitude. These same criteria and trends were discussed in Ref. 7 where the range of G for bounded trim angle near resonance was established.

The behavior of the slow circular frequency ω_s [Eq. (34)] within the resonance region is responsible for the static instability which occurs. The relation given below, derived by substituting Eqs. (12-16) into Eq. (34) and assuming that λ_p and $\lambda_y \approx 1$, demonstrates this behavior, as a function of G and λ_p, in or near the resonance region.

$$\omega_s = -p_{crp}\left\{ \frac{\left[\frac{1}{G^2} - \lambda_p^2\right](1-\lambda_p^2)}{\lambda_p^2\left[\frac{I_Y I_Z}{(I_Z-I_X)(I_Y-I_X)} + 1\right] + \frac{I_Y}{G^2(I_Z-I_X)} + \frac{I_Z}{(I_Y-I_X)}} \right\}^{1/2} \qquad (43)$$

Equation (43) shows that in the region between the undamped resonances ($\lambda_p = 1$ and $\lambda_y = G\lambda_p = 1$) ω_s is imaginary; on the boundaries of the region $\omega_s = 0$; and outside the region ω_s is real. With this information, it becomes obvious from Eqs. (28) and (29) that for vehicles with unsymmetrical static moment slope coefficients the m_2 and m_3 roots of Eq. (7) become real when the vehicle is flying in the region between the undamped resonances. In this region, the directions of the slow transient vectors become fixed; i.e., the circular frequency of these vectors is zero. When the magnitude of the ω_s term becomes larger than the magnitude of the negative λ_s term, one of the slow transient vectors diverges exponentially (static instability) while the other converges exponentially at a higher rate.

The damping rate λ_f of the fast transient vectors is unaffected by the occurrence of resonance. Near resonance, the fast frequency is given approximately by $\omega_f \approx 2(\Delta\omega)$, which is roughly twice the roll rate. The rotation direction of the fast rotating vectors remain unaltered throughout the flight regime. This is not true for the slow vectors which, in addition to having zero circular frequency between the resonances, have opposite rotation directions at super-resonant conditions (λ_p and $\lambda_y > 1$) than they do at subresonant conditions (λ_p and $\lambda_y < 1$). To illustrate these characteristics, the following relationships are used

$$\omega_f = (\omega_0 + \Delta\omega) + \frac{\omega_A}{2(\omega_0 + \Delta\omega)} - \ldots \qquad (44)$$

$$\omega_s = (\omega_0 - \Delta\omega) + \frac{\omega_A}{2(\omega_0 - \Delta\omega)} - \ldots \qquad (45)$$

These relationships, derived from Eqs. (33) and (34) using a binomial expansion, are valid when the term involving ω_A is small compared to one. This restriction is satisfied at conditions outside the resonance region. The sign of ω_f, Eq. (44), is unaltered by the relative magnitudes of ω_0 and $\Delta\omega$; however, this is not so for ω_s, Eq. (45). When $\Delta\omega > \omega_0$, as it does for λ_p and $\lambda_y > 1$, ω_s is negative. When λ_p and $\lambda_y < 1$, $\omega_0 > \Delta\omega$, and ω_s becomes positive. These behavior patterns were shown earlier in Ref. 3 for missiles with symmetrical stability derivatives. Pettus[8] used this characteristic behavior of the slow transient vector to describe the mechanism for re-entry vehicle oscillatory roll resonance.

For a missile with symmetrical stability derivatives, ω_s goes to zero at the coincident pitch and yaw resonances; however, the damping rate λ_s of the slow transient vector remains unaltered. As shown in Fig. 3 for $G = 1.0$, the presence of aerodynamic damping ($\mu_p \mu_y > 0$) prevents static instability. As indicated earlier in the discussion of Eq. (34), the basic difference between the slow frequency expressions for vhicles with unsymmetrical stability derivatives and those for vehicles with symmetrical stability derivatives is the presence of the ω_A term and the averaging of the unequal B_α and B_β coefficients which occurs. These added effects of unsymmetrical stability derivatives are responsible for the changes in the behavior of ω_s which cause static instability.

Numerical Analysis

The preceeding theoretical development provides an analytical tool by which a more complete knowledge can be gained concerning the effects of unsymmetrical stability derivatives on the transient angular motions of slender rolling re-entry vehicles. These quasi-steady results indicate that: 1) the largest effect of unsymmetrical stability derivatives is that of unsymmetrical static moment slope coefficients ($C_{m_\alpha} \neq -C_{n_\beta}$); 2) the presence of unsymmetrical stability derivatives alters the motion, damping, and frequency sufficiently to invalidate the use of previous analytical results developed for vehicles with symmetrical stability derivatives; and 3) between the resonances, when differences in C_{m_α} and C_{n_β} exceed some altitude-dependent limit, a rolling re-entry vehicle can become statically unstable. In order to establish the accuracy of the analytical expressions for the complex roots of the characteristic equation (damping and frequency expressions), comparisons were made at given flight conditions with complex roots obtained through a numerical analysis of the equation. Simulations obtained by numerically integrating the complete 6-DOF equations of motion were used to investigate the analytically predicted trends of static instability. Results of these numerical analyses are presented in this section.

The reference vehicle used for the frequency and damping comparisons and re-entry simulations was the Sandia Re-entry Vehicle Resonance Test Vehicle (RVRTV), a 10° half

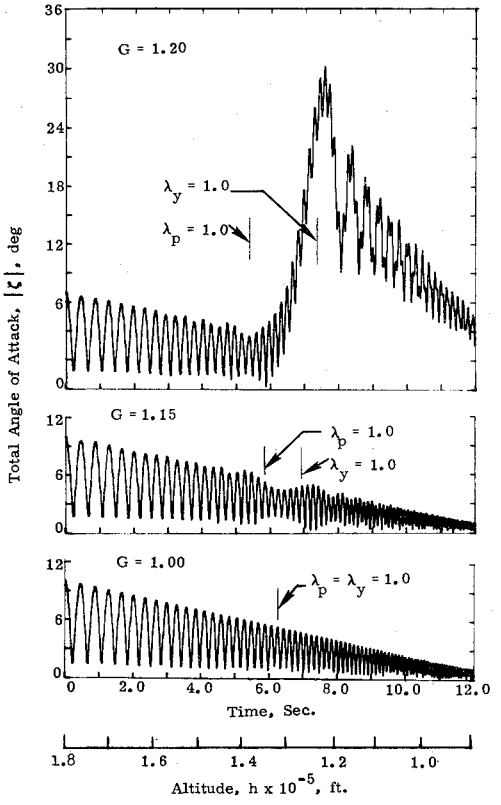

Fig. 4 Simulated (6-DOF) total transient angle-of-attack response to static moment slope asymmetry.

angle cone having a 1.25 ft (0.381 m) base diameter, a nose to base radius ratio of 0.0167, a 6% hypersonic static margin, and a Newtonian ballistic coefficient of approximately 1100 lb/ft^2 (5.267×10^4 N/m^2). The external geometry of this vehicle is the same as standard dynamic stability calibration models used by the Supersonic Tunnel Association and the AGARD.[10] The initial re-entry conditions used for the vehicle's reference trajectory were $U_i = 21{,}600$ fps (6584 m/sec), $\gamma_i = -20.6°$, $h_i = 180{,}000$ ft (54,864 m), $p_i = 18.85$ rad/sec, and $\alpha_i = 10°$. For these simulations and comparisons, the vehicle was symmetrical except for differences in C_{m_α} and C_{n_β}. The aerodynamic stability derivatives were kept constant to be consistent with the restrictions on the theory.

In Table I, analytical results for the damping and frequency of a slow transient vector are compared over a wide range of altitude with results obtained from a numerical analysis of the characteristic equation [Eq. (7)]. The comparison was made for an RVRTV with static moment slope asymmetries $G = 1.15$ ($C_{m_\alpha} \approx -1.3\, C_{n_\beta}$) that was flying along the reference trajectory. The accuracy of the analytical results is demonstrated by the excellent agreement with the results of the numerical analysis. The damping rate λ_s compares exactly to more than five significant figures over the complete altitude range, while the comparison for the circular frequency ω_s shows the analytical results to be accurate within 0.2% down to an altitude of 25,000 ft (7620 m). An even more favorable comparison is obtained when components of a fast transient vector are used. For example, the analytical expression for ω_f is accurate to within 0.04% over the complete altitude range used in Table 1. The analytically derived values of λ_f, like those of λ_s, compare exactly to more than five significant figures for these conditions. When effects of asymmetries in the force slope coefficients and damping derivative coefficients are included, the accuracy of the analytical expressions remain unchanged.

A description, based on results obtained from the 6-DOF simulations, is given in Fig. 4 of effects that unsymmetrical static moment slope characteristics ($G^2 = -C_{m_\alpha}/C_{n_\beta} > 1$, Fig. 4) have on the transient angular motion of a slender rolling re-entry vehicle. The high altitude resonance encounters shown in Fig. 4 were obtained for an RVRTV which had no trim producing asymmetries; i.e., F_α and F_β of Eqs. (1) and (2) were zero. The $G = 1.0$ curve in Fig. 4 is the reference curve since it represents the transient angular motion behavior of a vehicle with symmetrical stability derivative characteristics. The roll rate remained constant throughout these simulated flights because the roll torque, M_X was set equal to zero. Simulations like those shown in Fig. 4 provide a severe test of the quasi-steady analytical predictions because of the highly transient nature of the resonance encounters.

The 6-DOF results shown in Fig. 4 confirm the analytical predictions concerning the effects of unsymmetrical static moment slope characteristics on transient angular motion. The analytical results predict: 1) outside the region between the undamped resonances ($\lambda_p = 1$ and $\lambda_y = G\lambda_p = 1$) the motion converges, and 2) between the undamped resonances when $\theta_2 < 0$ [Eq. (39)], one slow transient vector diverges while the other converges at a more rapid rate. These behavior patterns are evident at this high altitude resonance encounter (Fig. 4) where the theory [Eq. (42)] predicts the vehicle to be unstable for $G < 0.986$ and $G > 1.014$. As shown by the $G = 1.15$ curve in Fig. 4, between the resonances the motion initially converges, then diverges. This divergence, which terminates as the vehicle passes out of the resonance region, causes the magnitude of the total angle of attack to become slightly greater than that of the $G = 1.0$ reference curve (Fig. 4) at the corresponding time. Because of the effect of transient resonance (roll rate constant—critical frequencies varying), relatively large values of static moment slope asymmetry are required to produce an explosive divergence in total transient angle of attack within the resonance region. When G is increased to 1.20 (Fig. 4) the static instability persists for a time sufficiently long to cause a large, possibly catastrophic divergence in total transient angle of attack. During this resonance encounter, the presence of the fast transient vectors is evident from the oscillating signal ($\omega_f \approx 2p$ near resonance) superimposed on the diverging slow transient vector.

Although the simulations presented in Fig. 4 confirm the analytical predictions, they contain some small additional effects not predicted by the theory. These effects cause minor changes in the total angle-of-attack envelope at conditions slightly above and slightly below resonance. They also cause the changes predicted by the theory to lead the initial undamped resonance crossing and to lag the final crossing. The theoretically derived conditions for the onset and termination of static instability were obtained directly from the characteristic equation of the dynamic system [Eq. (7)] without introducing approximations. Because of this, it is speculated that the additional effects observed in the 6-DOF simulations are caused by small terms which were neglected as small perturbations in the derivation of the linearized equations of motion [Eqs. (1) and (2)]. These additional small effects do not alter the fact that the linear theory derived from Eqs. (1) and (2) is a valuable tool for predicting the essential features of what could be a serious flight instability.

The results presented thus far, and those presented in Ref. 7, make it obvious that the angular motion behavior of a vehicle with unsymmetrical stability derivative characteristics cannot be modeled accurately or interpreted correctly through the use of analytical models developed for vehicles with symmetrical stability derivative characteristcs. If average values of the unsymmetrical stability derivatives are used and the vehicle is assumed to be symmetrical, unrealistic evaluations of the vehicles motion result (particularly near resonance) when static moment slope asymmetry is present. At conditions away from resonance, use of a symmetrical model to interpret data will result in an erroneous evaluation of any unsymmetrical stability derivatives.

Conclusions

A quasi-steady analytical theory has been developed which describes the effects that unsymmetrical stability derivative characteristics have on the transient angular motion behavior of slender rolling re-entry vehicles. Results presented in this article indicate that asymmetries in the static moment slope coefficients introduce the largest and most important changes in the transient angular motion behavior. Beside changing the angular motion patterns and the frequency and damping expressions, unsymmetrical static moment slope characteristics have important effects on the stability or lack of stability of the transient angular motion within the resonance region. Specific conclusions that can be drawn from the results presented here are as follows. 1) Static instability (exponential divergence of a total transient angle of attack component) occurs for flight conditions between the resonances when differences in the static moment slope coefficients exceed some altitude and aerodynamic damping dependent limit. 2) With unsymmetrical static moment slope characteristics the possibility of large trajectory dispersions and catastrophic vehicle failure exists because of the exponential divergence in transient angle of attack which can occur near resonance. 3) Because of the basic changes unsymmetrical stability derivatives introduce into the total transient angle-of-attack behavior, analytical models developed for vehicles with symmetrical stability derivative characteristics fail to predict the motion patterns and cannot be used to extract even averages of the unsymmetrical stability derivatives from data.

References

[1] Nicolaides, J. D., "On the Free-Flight Motion of Missiles Having Slight Configurational Asymmetries," Report 858, June 1953, U.S.

Army Ballistics Research Laboratory, Aberdeen Proving Ground, Md.

[2]Murphy, C. H., "Free flight Motions of Symmetric Missiles," Report 1216, July 1963, U.S. Army Ballistics Research Laboratory, Aberdeen Proving Ground, Md.

[3]Nelson, R. L., "The Motions of Rolling Symmetrical Missiles Referred to a Body-Axis System," NACA TN-3737, Nov. 1956.

[4]Phillips, W. H., "Effect of Steady Rolling on Longitudinal and Directional Stability," NACA TN-1627, June 1948.

[5]Regan, F. J., "Static and Dynamic Stability of Free-Fall Stores with Freely Spinning Stabilizers," NOLTR-73-19, Jan. 1973, Naval Ordnance Laboratory, While Oak, Silver Spring, Md.

[6]Walchner, O., "Asymmetric Nose Bluntness Effects on the Aerodynamics of a Slender Cone at Mach 14," *AIAA Journal*, Vol. 10, Aug. 1972, pp. 1121-1122.

[7]Hodapp Jr., A. E., "Effects of Unsymmetrical Stability Derivative Characteristics on Re-Entry Vehicle Trim Angle of Behavior," *Journal of Spacecraft and Rockets*, Vol. 11, May 1974, pp. 300-307.

[8]Pettus, J. J., "Persistent Re-Entry Vehicle Roll Resonance," AIAA Paper 66-49, New York, 1966.

[9]Etkin, Bernard, *Dynamics of Flight Stability and Control*, Wiley, New York, 1959.

[10]Fail, R. and Garner, H. C., "Calibration Models for Dynamic Stability Tests," AGARD Report 563, 1968, France.